View metadata, citation and similar papers at core.ac.uk
brought to you by CORE
provided by Digital Repository @ Iowa State University

PREDICTION OF THE PROBABILITY OF EDDY CURRENT FLAW DETECTION

R. E. Beissner,
K. A. Bartels, and
J. L. Fisher

Southwest Research Institute
6220 Culebra Road
San Antonio, Texas 78284

INTRODUCTION

The validity of a nondestructive inspection method can be measured by two quantities, the probability that a given flaw size will be detected, and the probability that background noise will give rise to a false indication of the presence of a flaw. Unfortunately, experimental determination of the probability of detection (POD) and the probability of false alarm (PFA) requires a rather extensive set of measurements to obtain statistically sound estimates. Furthermore, if one or more of the parameters that define the method, such as the scan track spacing or probe configuration, are changed, then the full set of measurements must be repeated to obtain new estimates of the POD and PFA, thus adding to the time and expense of test validation. In some situations, where one is designing an inspection for a part or flaw size that is not yet available for testing, there is no way that the validity of a proposed inspection can be evaluated beforehand.

There is, therefore, a need for reliable theoretical methods for predicting the probability of flaw detection. The most straightforward approach to POD prediction, and the one followed here, is to simulate, on a digital computer, the measurements one would make in an experimental determination. In general, this approach requires that one have available reliable methods for predicting flaw signals and background noise as a function of flaw size and shape, probe configuration and other inspection parameters. For eddy current testing, which is of concern here, not all of these requirements can be satisfied at present, and it is therefore necessary to supplement theoretical predictions with experimental data where theory is inadequate. However, existing eddy current theory is sufficiently advanced so that POD predictions can be made using experimental data only for noise statistics and normalization of predicted flaw signals. Accordingly, the principal purpose of the present work was to demonstrate such an application of theory and experiment to POD prediction. It should be noted that a similar demonstration has been previously reported [1], though the methods employed in that work differ from those reported here.

Methods used to generate the signal and noise data needed for POD predictions are outlined in the next section. This is followed by descrip-

tions of computer simulation computations leading to signal amplitude probability distribution functions, and, in the final section, calculated POD and PFA data for four flaw sizes.

BASIC CALCULATIONS AND EXPERIMENTS

The inspection geometry is illustrated in Fig. 1. Four flaws, in the form of rectangular slots, were investigated; the flaw dimensions were 0.25 mm (length) by 0.12 mm (depth), 0.5 by 0.25 mm, 0.75 by 0.37 mm, and 1.0 by 0.5 mm. Flaws were oriented with lengths parallel to the probe scan direction, which was the y axis of Fig. 1. An absolute, air-core, cylindrical probe was used with outer diameter 1.8 mm, winding thickness 0.25 mm, and winding length 0.25 mm; the frequency was 1.7 MHz. The parameter d shown in Fig. 1 is the distance from the flaw to the nearest scan track. This distance was treated as a random variable in the POD calculations, i.e., it was assumed that variability in the flaw signal was caused by variations in the position of the flaw with respect to a scan track.

Given this geometry, calculation of the POD requires data on the dependence of the flaw signal on the parameter d as the probe is scanned past the flaw in the y direction of Fig. 1. Because d can have any value from zero to one-half the scan track spacing, the requirement is, in effect, for a map of the probe response as a function of d and y. It is important to note that, except in rare cases where the flaw length is much greater than the probe diameter, the problem posed by this requirement is inherently three-dimensional, i.e., the need for a realistic y-d map dictates a three-dimensional model of the probe and flaw geometries.

In the present work the y-d map was provided by an eddy current version of the boundary element method [2] and application of the reciprocity theorem [3]. The reciprocity theorem, in the form used here, relates the probe impedance change caused by the flaw to fields on the flaw surface as follows:

$$\Delta Z = C \int (\vec{E}_R X \vec{H}_T - \vec{E}_T X \vec{H}_R) \cdot \vec{n} dS, \qquad (1)$$

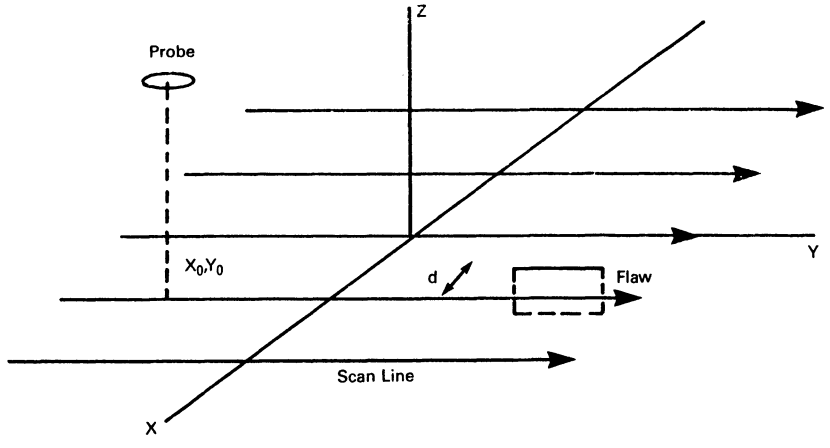

Fig. 1. Geometry chosen for simulation of an eddy current test. The surface of the test piece is the x,y plane. The flaw is a rectangular slot at the surface and located a distance d from the nearest scan line.

where ΔZ is the impedance change, $\vec{E}$ and $\vec{H}$ are electric and magnetic fields, C is a calibration constant to be determined, and the integral is over the flaw surface. The subscripts T and R refer to fields on the flaw surface and fields in the absence of the flaw, respectively.

The R fields in Eq. (1) were calculated from an analytic solution [4] of Maxwell's equations which, in the present case, is equivalent to the Dodd and Deeds solution [5]. The T fields were calculated by the boundary element method, which results in a solution of the form

$$\begin{pmatrix} \vec{E}_T \\ \vec{H}_T \end{pmatrix} = Z^{-1} \begin{pmatrix} \vec{E}_0 \\ \vec{H}_0 \end{pmatrix}, \tag{2}$$

where the $\vec{E}$ and $\vec{H}$ variables now represent column vectors that give the values of the corresponding fields on an array of nodal points on the flaw surface, $\vec{E}_0$ and $\vec{H}_0$ are incident fields in the absence of the flaw (the same as $\vec{E}_R$ and $\vec{H}_R$ for an absolute probe), and Z^{-1} is the solution matrix defined in Ref. 2. Because the solution matrix depends only on the flaw geometry and skin depth, it is independent of probe position and need be computed only once for an entire y-d map of probe response.

The procedure for computing the flaw response map for each flaw size was therefore as follows: for each probe position (y,d) with respect to the flaw, (1) compute the fields $\vec{E}_0 = \vec{E}_R$ and $\vec{H}_0 = \vec{H}_R$ by numerical evaluation of the integral solution given in Ref. 4; (2) apply Eq. (2) to determine the flaw surface fields $\vec{E}_T$ and $\vec{H}_T$; and (3) numerically evaluate the integral in Eq. (1) to determine a complex number proportional to ΔZ.

Figure 2 is a plot of the amplitude of ΔZ as a function of position with respect to the 0.5 by 0.25 mm flaw, which is located at the center of the picture. The area covered in this display is 2.5 by 2.5 mm, and the

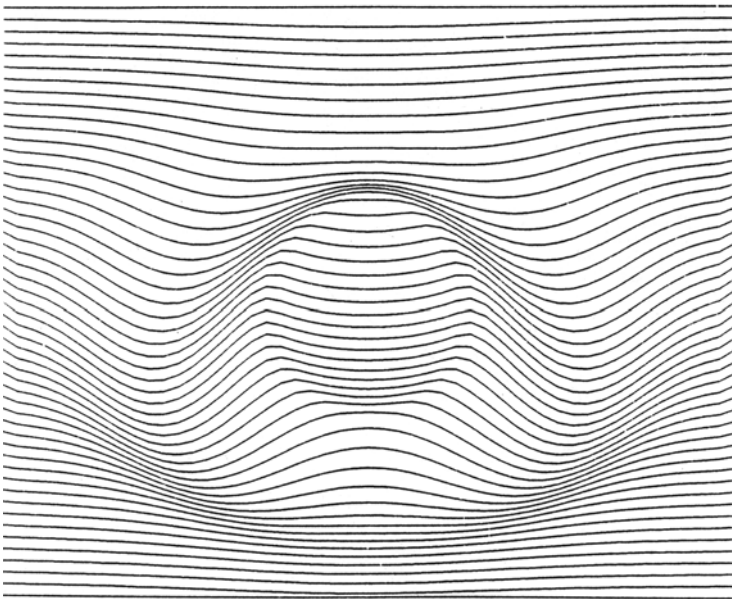

Fig. 2. Calculated amplitude of the flaw signal as a function of probe coordinates x_0, y_0 of Figure 1. The flaw is a 0.5 by 0.25 mm slot at the center (x=0,y=0) of the figure. Amplitude peaks form a circular pattern with diameter approximately equal to the probe diameter (1.8 mm).

spacing between scans is 0.05 mm. Phase data were used to construct a similar map, which is not shown here.

Experimental data were obtained for the same array of EDM slot sizes in a titanium alloy plate, using an absolute probe of approximately the same dimensions at approximately the same frequency as in the calculations. The amplitude data for the largest (1.0 by 0.5 mm) slot are shown in Fig. 3. As can be seen from this figure, the experimental data are very noisy. This was deliberate; no attempt was made to reduce the noise by standard techniques such as signal averaging because a situation of marginal detectability was desired for comparison with POD predictions. As a result, plots similar to Fig. 3 for the two smallest flaws showed no visual evidence of flaw signals.

In addition to the flaw signal maps, experimental data were also obtained on background noise by means of a series of 41 scans in an area well away from the flaw locations. These data, and the flaw signal data shown in Fig. 3, were used to calibrate the predicted signals according to the formula

$$(Z_0 + \Delta Z)_{exp} = Z_0 + \Delta Z_{th}, \tag{3}$$

where $(Z_0 + \Delta Z)_{exp}$ is the measured signal at the point of maximum amplitude from the data in Fig. 3; Z_0 is the signal in the absence of a flaw, which was taken to be the average impedance observed in the background data; and ΔZ_{th} is the predicted signal given by Eq. (1), including the calibration constant C. On the assumption that C is a real number, this equation was solved for C to fix the normalization of predicted flaw signals.

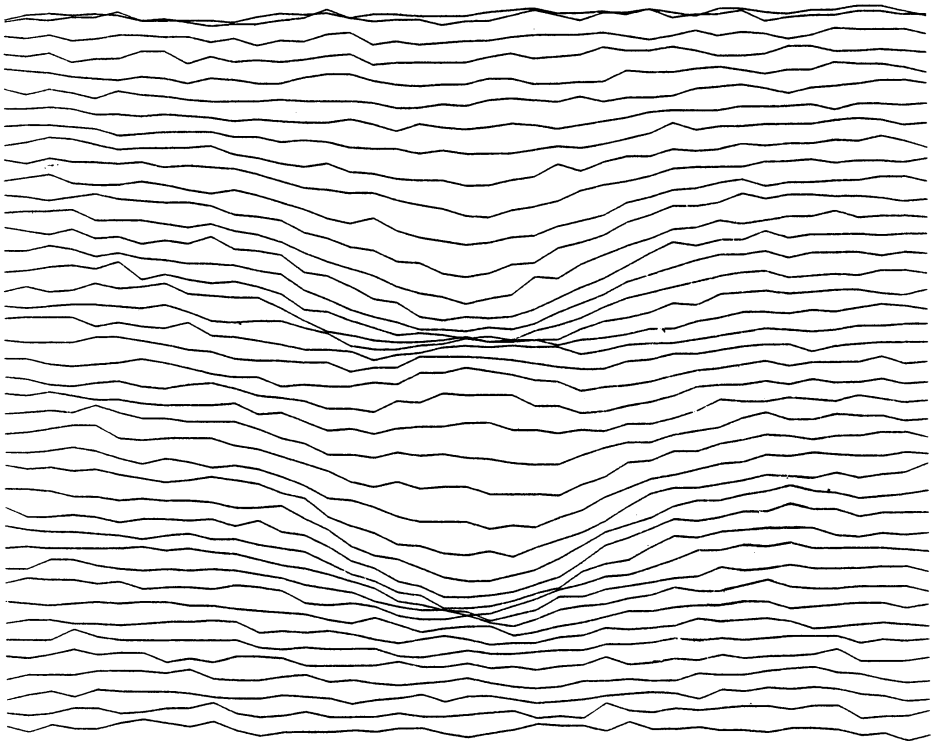

Fig. 3. Experimental amplitude map for a 1.0 by 0.5 mm slot. The area covered here is slightly larger than that of Figure 2.

COMPUTER SIMULATION

When the "no flaw" signal Z_0 is added to the normalized impedance change ΔZ given by Eq. (1), the result is a prediction of the complex flaw signal as a function of probe position. The addition of measured impedance fluctuations in the absence of a flaw (noise) therefore provides the data needed for a computer simulation of an eddy current test.

To enhance flaw detection it is now common practice to first determine the trajectory of noise signals in the complex impedance plane, and then look for components of the flaw signal orthogonal to the noise line. Given the calculated complex signal data and measured noise data described above, one could simulate this so-called quadrature method of flaw detection on the computer. However, for the sake of simplicity, this was not done in the present work. Instead, the simulation described below was based only on signal amplitude, making no use of calculated or measured phase changes.

The simulation of a series of eddy current tests was carried out as follows: (1) from normalized data like that shown in Fig. 2, determine the maximum signal amplitude in a scan at a fixed distance d; (2) repeat step (1) for a large number (10,000) of d values ranging from zero to one-half the scan track spacing; (3) record the number of times a peak flaw signal falls within each of 100 equally spaced amplitude intervals; (4) divide the numbers recorded in step (3) by the total number of histories (10,000) to obtain a signal amplitude probability distribution, i.e., probability density vs. signal amplitude. These steps were carried out for each of the four flaw sizes and also for the experimental noise data to determine the noise amplitude probability distribution. In the data described below, the scan track spacing was taken as 2.7 mm, which is one and one-half times the probe diameter.

A typical result is shown in Fig. 4 for the 0.5 by 0.25 mm slot. For this particular flaw size, the figure shows that the minimum signal amplitude lies near the center of the noise distribution, while the maximum signal amplitude, which would be realized when the flaw lies directly under or very near a scan line, lies above the maximum noise amplitude. This means that under favorable conditions, when the flaw is close to a scan line, the flaw signal should be recognizable. Conversely, signals corresponding to flaws at greater distances from a scan line may be too weak to distinguish from noise. Data for the other flaw sizes show the expected trend--the signal distribution function is compressed to the left for smaller flaws and expanded to the right for larger flaws, with the minimum signal amplitude remaining fixed at the point shown in Fig. 4.

POD PREDICTIONS

The interpretation of eddy current test data involves the decision as to whether an observed signal fluctuation is a flaw signal or noise. The simplest approach to making this decision is to choose some threshold signal level such that all signals above that level will be considered flaw signals and all signals below the level will be interpreted as noise. If the signal and noise probability distribution functions (PDFs) overlap, as in Fig. 4, then data interpretation based on threshold detection will inevitably involve error. In general, there will be a nonvanishing probability that a flaw is missed because its signal is below the threshold, and another probability that a noise fluctuation is incorrectly interpreted as a flaw indication because it is above the threshold.

Given the signal and noise PDFs, one can determine how the probability of flaw detection (a signal is correctly interpreted as a flaw indication)

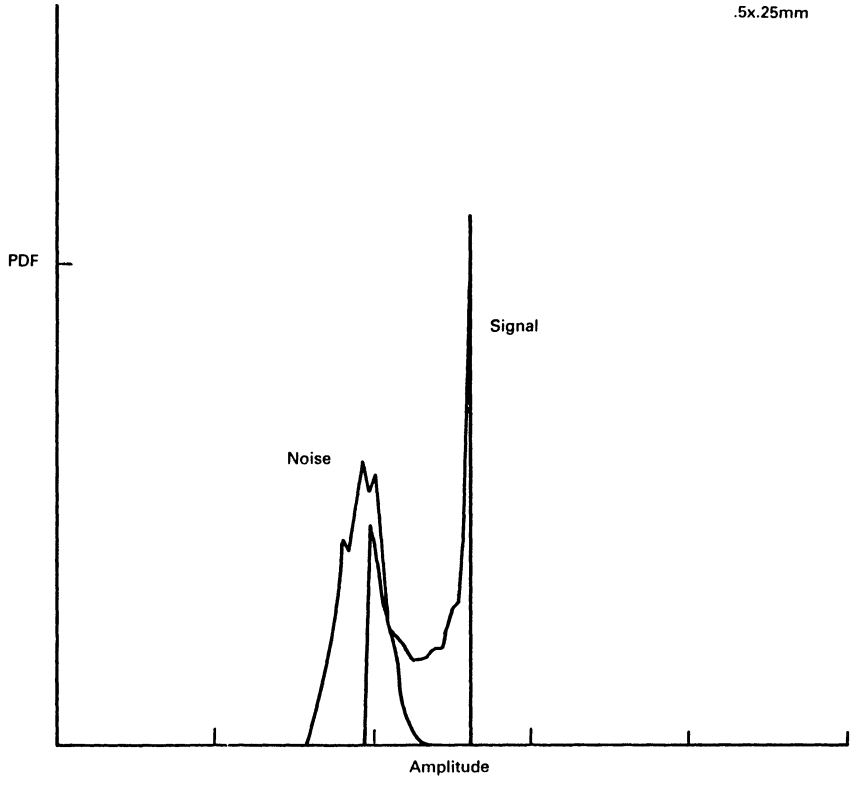

Fig. 4. Probability distribution functions for noise and the calculated signal from a 0.5 by 0.25 mm slot.

and the probability of false alarm (a signal is incorrectly interpreted as a flaw indication) depend on the choice of the threshold signal. This is illustrated schematically in Fig. 5, which shows that the detection probability (POD) is the area to the right of the threshold under the signal PDF curve, while the false alarm probability (PFA) is the corresponding area under the noise PDF. By choosing a number of different threshold values, one can generate a set of ordered pairs of POD and PFA values, which comprise the so-called operating characteristic of the inspection. The significance of the operating characteristic is that it defines the

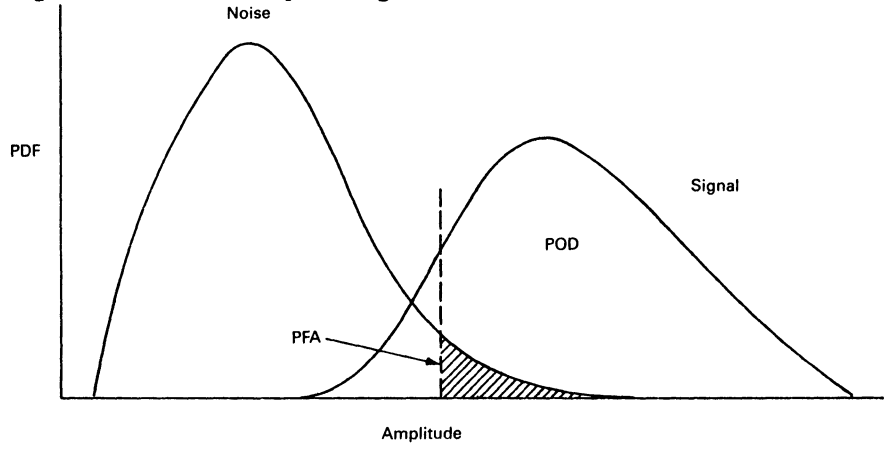

Fig. 5. Schematic illustration of the calculation of the probability of detection (POD) and the probability of false alarm (PFA).

tradeoff one must make between the efficiency of flaw detection, as measured by the POD, and the chance of rejecting a part that has no flaw, as measured by the PFA. In this sense, the operating characteristic is a concise statement of the validity of an NDE inspection.

Figure 6 contains plots of the operating characteristics for the four flaw sizes considered in this work. The results agree with the qualitative judgments one would make from observation of the experimental results for known flaws. Thus, Fig. 6 shows that for the largest flaw (1.0 by 0.5 mm), a high probability of detection can be achieved along with a low probability of false alarm. For the smaller flaws, on the other hand, one must tolerate a higher probability of false calls in order to realize a high probability of flaw detection. In fact, for the two smallest flaws, to achieve a POD approaching 1.0 one must set the threshold so low that about half the signal fluctuations associated with noise will be falsely interpreted as flaw indications. In other words, the two smaller flaws are virtually undetectable, in agreement with experimental observation.

CONCLUSION

The work reported here demonstrates that one can use theoretical predictions to analyze the validity of an eddy current test. Given a three-dimensional model of the probe/flaw interaction, such as the boundary element model used here, and supplementary experimental data for normalization and noise analysis, a large number of eddy current tests can be efficiently simulated on the computer to provide the data needed for probability of detection predictions.

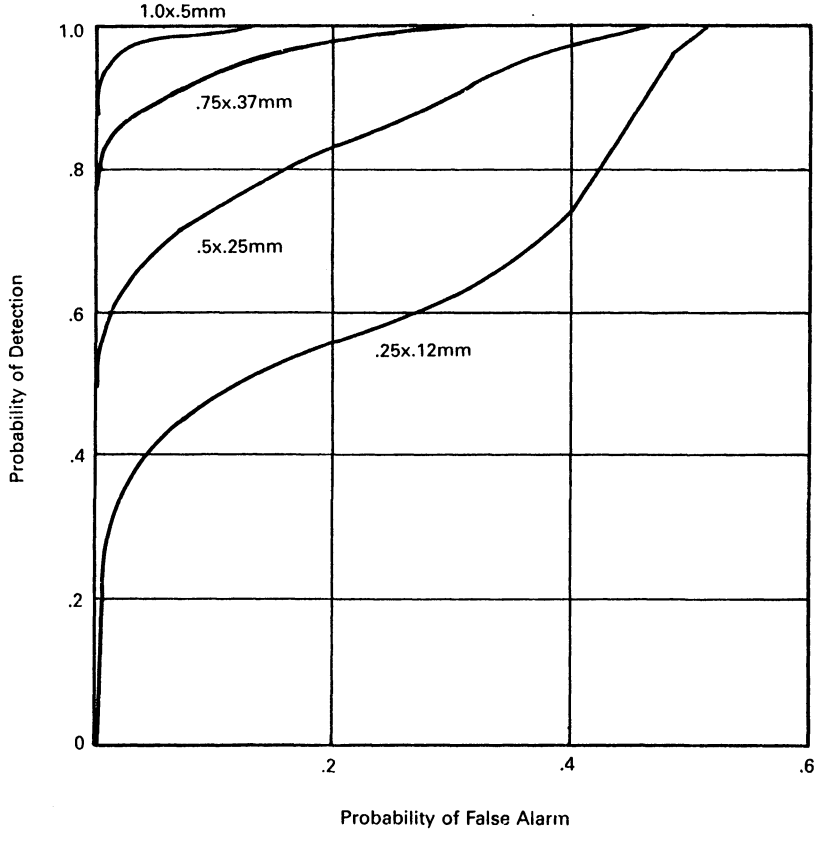

Fig. 6. Predicted operating characteristics for four slot sizes.

ACKNOWLEDGEMENT

This work was supported by the Center for Advanced Nondestructive Evaluation, operated by Ames Laboratory, USDOE, for the Air Force Wright Aeronautical Laboratories/Materials Laboratory under Contract No. W-7405-ENG-82 with Iowa State University.

REFERENCES

1. J. R. Martinez and A. J. Bahr, "Statistical Detection Model for Eddy-Current Systems," Review of Progress in Quantitative NDE, Vol. 3A, D. O. Thompson and D. E. Chimenti, eds., Plenum, New York (1984), p. 499.

2. R. E. Beissner, "Boundary Element Model of Eddy Current Flaw Detection in Three Dimensions," J. Appl. Phys. 60, 352 (1986).

3. B. A. Auld, "Theoretical Characterization and Comparison of Resonant Probe Microwave Eddy Current Testing with Conventional Low Frequency Eddy Current Methods," in "Eddy Current Characterization of Materials and Structures," ASTM STP 722, G. Birnbaum and G. Free, eds., American Society for Testing and Materials, Philadelphia (1981), p. 332.

4. R. E. Beissner and M. J. Sablik, "Theory of Eddy Currents Induced by a Nonsymmetric Coil Above a Conducting Half-Space," J. Appl. Phys. 56, 448 (1984).

5. C. V. Dodd and W. E. Deeds, "Analytical Solutions to Eddy-Current Probe-Coil Problems," J. Appl. Phys. 39, 2829 (1968).